



# Kinetics of melt crystallization of organic eutectic forming binary mixtures in non-flow systems

K.B. Radhakrishnan<sup>a</sup>, A.R. Balakrishnan<sup>b,\*</sup>

<sup>a</sup> Department of Chemical Engineering, T.K.M. Engineering College, Kollam 691 005, Kerala, India

<sup>b</sup> Department of Chemical Engineering, Indian Institute of Technology Madras, Chennai 600 036, India

Accepted 6 May 2000

## Abstract

The kinetics of melt crystallization of binary eutectic forming organic mixtures in non-flow systems with cooling from below for the preferential crystallization of one component alone have been studied experimentally. The effect of subcooling, superheating and the initial concentration of the melt on the crystallization kinetics have been studied. Based on the experimental data, a correlation for the instantaneous height of the crystal (volume fraction of the solidified mass) has been proposed. The experimental results were also analyzed based on a model from the literature, which considered simultaneous heat and mass transport. The analysis shows that in the present experiments, the melt crystal interface was very close to the initial melt composition, i.e. concentration equilibrium was maintained. This is attributed to the very low cooling rates used, even though the thermal diffusivity is much greater than the mass diffusivity of the melt. © 2001 Elsevier Science B.V. All rights reserved.

*Keywords:* Melt crystallization; Subcooling; Thermal diffusivity

## 1. Introduction

Melt crystallization is a process for the separation of a binary mixture of organic compounds. It is the process where a molten mixture is cooled to a little below its freezing point when some of the material solidifies. In binary mixtures, that form a eutectic, this will be a pure component. The remaining melt, called the residue, will contain some of the unsolidified pure (desired) component. The purified product is recovered by separating the solid from the residue and remelting it. It is an attractive method for separation of binary organic mixtures where the boiling points of the two components are very close to each other and distillation is not so easy. This is distinct from the solid solution systems where the phase diagram is similar to the vapor liquid equilibrium diagram of ideal systems. Unlike the eutectic forming systems, the crystal phase growing in equilibrium with the liquid of a given composition is not a pure substance and hence multistage operations are required to attain high purities.

Wynn [1] has classified melt crystallization processes into two categories — suspension processes and progressive freezing. In suspension processes the crystals are suspended in the melt and the density difference between crystals and melt causes a relative counter-current motion between the two. Progressive freezing, a technique unique to melt crystallization, involves the growth of the crystal layer on a cold surface immersed in the melt. The rather limited literature on melt crystallization has been reviewed by Ulrich [2] and Rittner and Steiner [3].

The kinetics of melt crystallization (rate of crystal growth) is a basic characteristic of the process. The present study focuses on the separation of binary organic eutectic mixtures by melt crystallization in non-flow or stagnant systems. The experimental data obtained in the present study is used to examine the effect of subcooling, superheating and the initial concentration of the melt on the crystal growth rates. The experimental data was also used to develop empirical correlations for estimating the melt crystallization kinetics. The experimental results are also examined using a model from the literature based on heat and mass transfer theory.

\* Corresponding author. Tel.: +91-44-4458209; fax: +91-44-2350509.

E-mail address: arbala@acer.iitm.ernet.in (A.R. Balakrishnan).

Fig. 1 shows the phase change diagram of binary organic eutectic forming mixtures. If the initial composition of the melt is below the eutectic point, as it cools, it will reach the liquidus line when pure naphthalene (in the benzene–naphthalene system shown in Fig. 1a) will crystallize out. As further cooling proceeds the composition will move along the liquidus line, while pure naphthalene continues to crystallize out, until the eutectic point is reached. At this point no more separation is possible and the solid forming will be a mixture of the binary at the eutectic composition. Similar behavior is observed with other two systems.

## 2. Experimental

The experimental set-up consists of a test section and two auxiliary devices. These auxiliary devices are a circulating cooling bath with a temperature controller and a power supply unit. The test section is a vertical glass cylinder covered with a 50-mm-thick styrofoam insulation. The insulation could be easily removed to facilitate the visual observation of crystallization process as and when required. The plate at the bottom which serves as the heat transfer surface is made of brass and was provided with a circular groove so that the 3.5-mm-thick glass cylinder can fit exactly in it. Fig.

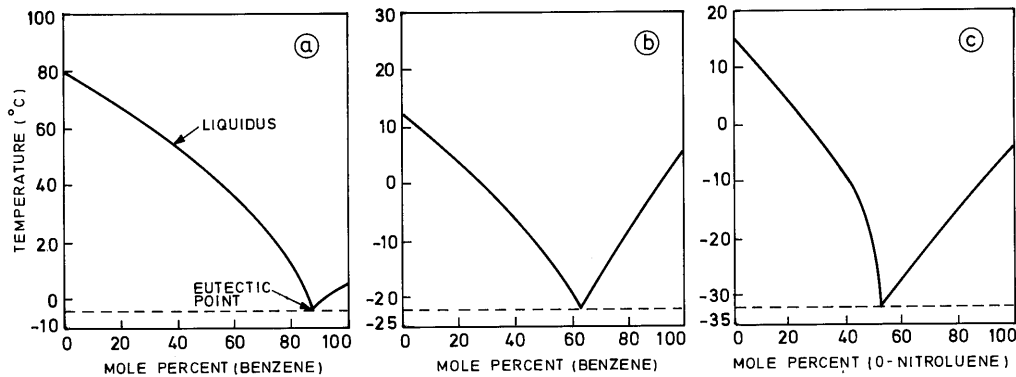


Fig. 1. Phase diagram of the binary mixtures, (a) benzene–naphthalene system; (b) benzene–*p*-xylene system; (c) *o*-nitrotoluene–*m*-nitrotoluene system.

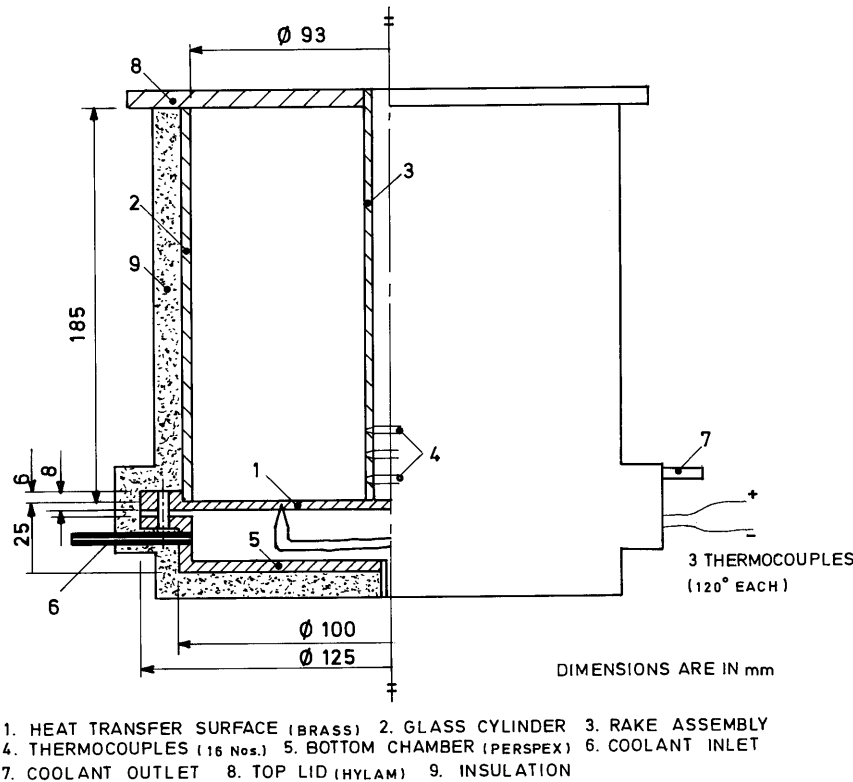


Fig. 2. Test section details.

Table 1  
Experimental conditions

Number	Binary system	Range of variables			$T_c$ (°C)	$C_l$ (mol%)
		$C_0$ (mol%)	$T_w$ (°C)	$T_0$ (°C)		
1	Naphthalene–benzene	20–25 Naphthalene	6–16	25–58	–3.5	87.5 Benzene
2	<i>p</i> -Xylene–benzene	2.5–10 <i>p</i> -Xylene	6–10	25–58	–22.2	62.7 Benzene
3	<i>m</i> -Nitrotoluene– <i>o</i> -nitrotoluene	5–15 <i>o</i> -Nitrotoluene	4–10	25–60	–31.5	52.0 <i>o</i> -Nitrotoluene

2 shows the details of the brass plate. Another cylindrical chamber made of Perspex and with an o.d. of 200 mm is attached to the bottom of the brass plate. This is tightly fitted to the brass plate with rubber gasket and bolts. The cooling water from the chiller flows through this bottom chamber. A rotameter and two control valves are used to regulate the flow rate of the cooling water through the chamber. The brass heat transfer surface between the cooling water and the melt is 2-mm thick. The test section itself is 93-mm i.d. and 185 mm high. The top of the cylinder was covered with a Hylam sheet, which fits tightly on to the cylinder. A thermocouple rake assembly is attached to this sheet at the center with 16 Teflon coated copper-constantan (type T) thermocouples. This is used to measure the temperature distribution of the melt/solid along the vertical direction from the cooling plate. The bottom plate has three thermocouples with a junction diameter of less than 1.5 mm, carefully embedded in the lower surface of the plate at approximately 120° from each other circumferentially. Highly conductive silicon paste was used to ensure good conduction between the beads and the cooling surface. The accuracy of the temperature measurement was  $\pm 0.1^\circ\text{C}$ . The liquidus temperature for each composition can be determined from the phase diagram (Fig. 1). The cooling water lines, the top and bottom of the test section were insulated with 50-mm-thick styrofoam insulation.

Experiments were performed at different initial concentrations, all of which were below the eutectic composition and at different values of subcooling and superheating of the melt. Table 1 gives a summary of the experimental conditions. In all the experiments, the surface temperature was maintained well above the eutectic temperature and above the crystallization temperature of the undesired product. This facilitates the separation of one component alone. At the beginning of each experiment, cooling water was circulated through the lower chamber to reduce the temperature of the heat transfer surface to the desired level. The binary melt at a known composition and temperature is then filled in the test-section (glass walled insulated cylinder above the heat transfer surface) upto a height of about 80 mm. During the filling process, a sudden

jump in the temperature of the heat transfer surface was noticed, but this was found to stabilize within about 2 min. The temperature of the heat transfer surface was kept constant throughout the experiments, and the variation observed was  $\pm 0.2^\circ\text{C}$ . The solidification process was observed to proceed from the bottom upwards with the crystal/melt interface parallel to the base and was morphologically stable. The instantaneous location of the crystal/melt interface was measured using a probe, which was a thin glass rod. The probe was immersed through a 4-mm hole on the top lid. Care was taken to avoid the formation of the impression of the rod on the crystal/melt interface. The formation of such impressions on the crystal surface leads to inhibition of further crystal growth at such locations and affects the measurements. The instantaneous location of the crystal/melt interface was also noted by observing the interface height measured from the bottom wall through the glass cylinder. This was done by removing a small strip of styrofoam insulation from the cylinder surface. The temperatures along the vertical axis were measured using the thermocouples provided on the rake at preselected heights from the bottom brass plate.

### 2.1. Standardization of the experimental set-up

To standardize the experimental set-up, experiments were conducted to measure the crystal/melt interface location using *p*-xylene without any initial superheat and at four different values of surface temperature. These were compared with the data of Hale and Viskanta [4], whose experiments were conducted using *n*-octadecane. In order to facilitate the comparison to one figure, the location of the interface as shown in Fig. 3 is represented by a dimensionless distance  $S$ , defined as

$$S = \frac{s(t)}{l} \quad (1)$$

where,  $l$  is the initial height of the liquid melt.  $S$  also gives the ratio of the volumes of the crystallized material to the total volume of the melt. The  $x$ -axis is represented by  $St\tau$ .  $\tau$ , a dimensionless time multiplied

by the Stefan number, thereby taking into account the thermophysical properties of the two binary materials. Good agreement can be observed in Fig. 4 between the present data and the data of Hale and Viskanta [4].

### 3. Results and discussion

#### 3.1. Morphological stability

The subcooling,  $T_1(C_0) - T_w$ , used in the experiments was carefully controlled to ensure a flat and planar surface. The surface temperature has to be kept below the crystallization temperature of the desired component but above that of the other component and well above the eutectic temperature of the binary mixture. This helps in the preferential crystallization of one

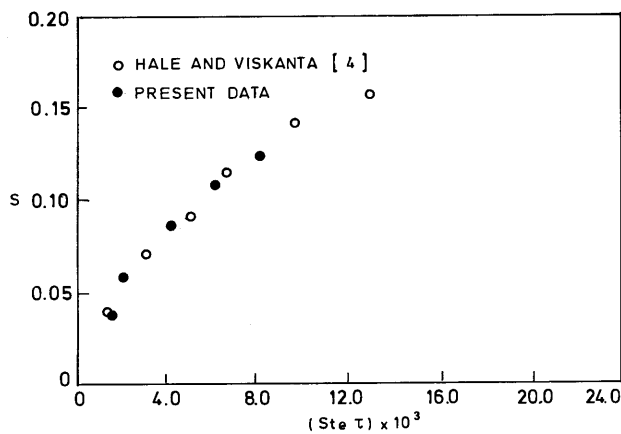


Fig. 3. Comparison to present data on crystallization of pure *p*-xylene with literature data on pure *n*-octadecane.

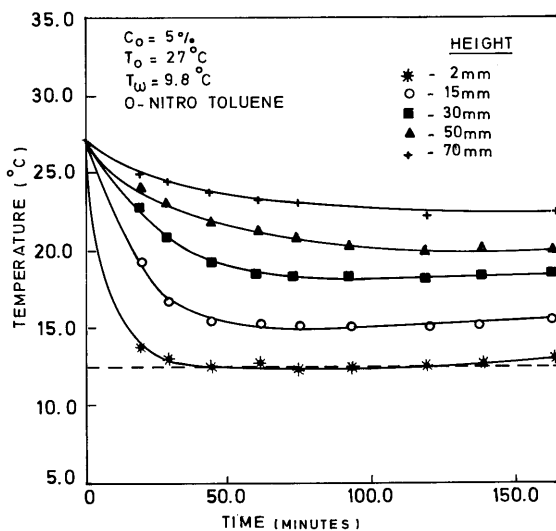


Fig. 4. Temperature trace with time at different locations during crystallization of the *o*-nitrotoluene-*m*-nitrotoluene system.

component alone without freezing of the undesired component entrapped within the crystal interstices. Furthermore, the instability at the interface due to constitutional supercooling (supercooling due to change in composition caused by the preferential solidification of one constituent) will lead to dendrite formation and this may in turn lead to crystallization of the undesired component. Worster [5] defined a criterion to avoid supercooling and subsequent linear instabilities at the interface (i.e. non-flat and non-planar interface)

$$k_s > \frac{k_m}{1 - [1 - (\lambda/\xi C p_s)(D/\alpha_s)(1/C_0)]} \quad (2)$$

where,  $\xi$  is the slope of the liquidus line and  $C_0$  is the initial composition of the melt. The above criterion was checked with the thermophysical, transport, phase equilibrium (solid-liquid) data and the experimental parameters used in the experiments and it was confirmed that linear instability would not be a problem in the present study. Furthermore, observations during the experiments also showed that there was no dendrite formation. The physical properties of the binary mixtures are given in Table 2.

#### 3.2. Free convection effects

The temperatures were measured at different locations in the test cell and are shown in Fig. 4. The random oscillations of temperature that can be expected from fluid motion driven by buoyancy effects were not noticed during the crystallization process, even when the initial melt superheat was as high as 13.5°C. This shows that free convection effects are minimum and conduction is the dominant mode of heat transfer. Furthermore, Worster [5] has pointed out that the bulk temperature and the solute fields are statistically stable to convective motion if the system is cooled at the lower horizontal boundary and if the less dense component is crystallized. In the systems studied in the present investigation, the less dense component was crystallized, except for the benzene-naphthalene system. However, even here free convection effects were not noticed. This is due to the crystal/melt interface being colder than the bulk melt above it. This was noticed visually also. In Fig. 5 the sudden drop in the melt temperature at the beginning of the experiment is due to the high thermal gradient, the melt was subjected to at the start of the experiment. This was because the surface temperature was kept slightly above the crystallization temperature of the melt prior to charging the melt. This was done to prevent the supercooling of the melt in the region adjacent to the cooling surface immediately on charging the melt into the container. The melt temperature was found to stabilize within the first 15 min.

Table 2  
Physical properties of the binary mixtures used

Properties $C_0$ (mol%)	Benzene–naphthalene		Benzene- <i>p</i> -xylene			<i>o</i> -Nitrotoluene- <i>m</i> -nitrotoluene		
	75% (benzene)	80% (benzene)	2.5% (benzene)	5% (benzene)	10% (benzene)	5% <i>o</i> -Nitrotoluene	10% <i>o</i> -Nitrotoluene	15% <i>o</i> -Nitrotoluene
$\rho_m$ (kg/m <sup>3</sup> )	917.6	913.5	861.11	862.3	863.6	1162.06	1162.36	1162.7
$C_{p_m}$ (J/kg K)	1679.9	1680.81	1677.43	1677.8	1678.0	1591.14	1591.14	1591.14
$k_m$ (W/m K)	0.190	0.198	0.133	0.135	0.135	0.138	0.138	0.138
$\mu_m \times 10^3$ (kg/m s)	0.810	0.798	0.667	0.669	0.673	2.566	2.567	2.571
$\lambda \times 10^{-5}$ (J/kg)	1.492			1.584			1.23	
$C_{p_s}$ (J/kg K)	1223.4			1679.84			1591.14	
$k_s$ (W/m K)	0.367			0.143			0.139	
$\rho_s$ (kg/m <sup>3</sup> )	1158			869			1174	
$D \times 10^9$ (m <sup>2</sup> /s)	1.218			1.457			0.361	

### 3.3. Crystal growth rates — effect of subcooling/superheating and initial concentration

Fig. 5a shows the height of crystal layer with time, using subcooling as a parameter. The crystal growth rate decreases with the progress of crystallization due to the additional resistance of the crystal layers. The crystallization rates were appreciably higher when the subcooling was raised from 2.5 to 12.5°C for the naphthalene–benzene system. Similar effects were noticed with the other two systems.

The growth rates of the crystal layers are shown in Fig. 5b with initial superheat as a parameter (with constant subcooling). The growth rate decreases with the increase in initial superheat, which is due to the higher cooling load that has to be met. However, it may be noted that the effect of superheat on crystallization rates is less pronounced than that of subcooling.

Fig. 5c shows the growth of the crystal layer at constant wall temperature, with initial concentration as parameter. The maximum crystal layer growth obtained was highest for the lower concentrations of non-crystallizing component (25 mol% naphthalene in benzene–naphthalene system, 2.5 mol% benzene in benzene–*p*-xylene system and 5 mol% *o*-nitrotoluene in *o*-nitrotoluene–*m*-nitrotoluene system). For lower concentrations of the non-crystallizing component, the higher equilibrium temperature results in a higher temperature driving force (or a higher subcooling) at a constant wall temperature.

## 4. Correlation of the experimental data

### 4.1. Transient crystal height

Using the experimental data on the kinetics of crystallization from the present study, the solid–liquid

phase equilibrium data, the transport and thermodynamic properties of the binary melt, a correlation in non-dimensional form for the height of the crystallized solid (transient crystal growth) for eutectic forming binary organic mixtures for low subcoolings (also called undercooling) has been developed

$$S = 1.77(Ste.\tau)^{0.5}(1 - Ste^*)^{0.88}(C'_0)^{-0.31} \quad (3)$$

where,  $Ste$ ,  $Ste^*$  and  $C'_0$  are the Stefan number, a modified Stefan number (degree of initial superheat) and a non-dimensional concentration, respectively. The ranges covered by the parameters are:

$$0.022 < Ste < 0.12 \quad 0.13 < Ste^* < 0.41$$

$$0.086 < C'_0 < 0.92$$

The Stefan number is defined as

$$Ste = \frac{C_{p_s}(T_l(C_0) - T_w)}{\lambda} \quad (4)$$

where,  $C_{p_s}$  is the specific heat of the crystallized component;  $T_l(C_0)$ , the liquidus temperature corresponding to the initial melt composition;  $T_w$ , the temperature of the cooled boundary; and  $\lambda$ , the latent heat of the crystallized material. Thus,  $Ste$  represents the ratio of the sensible heat of the crystal to the latent heat needed for phase change. The modified Stefan number is defined as

$$Ste^* = \frac{C_{p_m}(T_0 - T_l(C_0))}{\lambda} \quad (5)$$

$Ste^*$  represents the ratio of the sensible heat (initial superheat) of the melt to the latent heat needed for phase change. The non-dimensional concentration is defined as

$$C'_0 = \frac{|C_e - C_0|}{C_e} \quad (6)$$

$C'_0$  represents the non-dimensional melt composition. Here  $C_0$  is the initial melt composition and  $C_e$  is the

eutectic composition. This dimensionless number gives the relative concentration difference of the initial composition to the eutectic composition. The performance of the correlation is shown in Fig. 6.

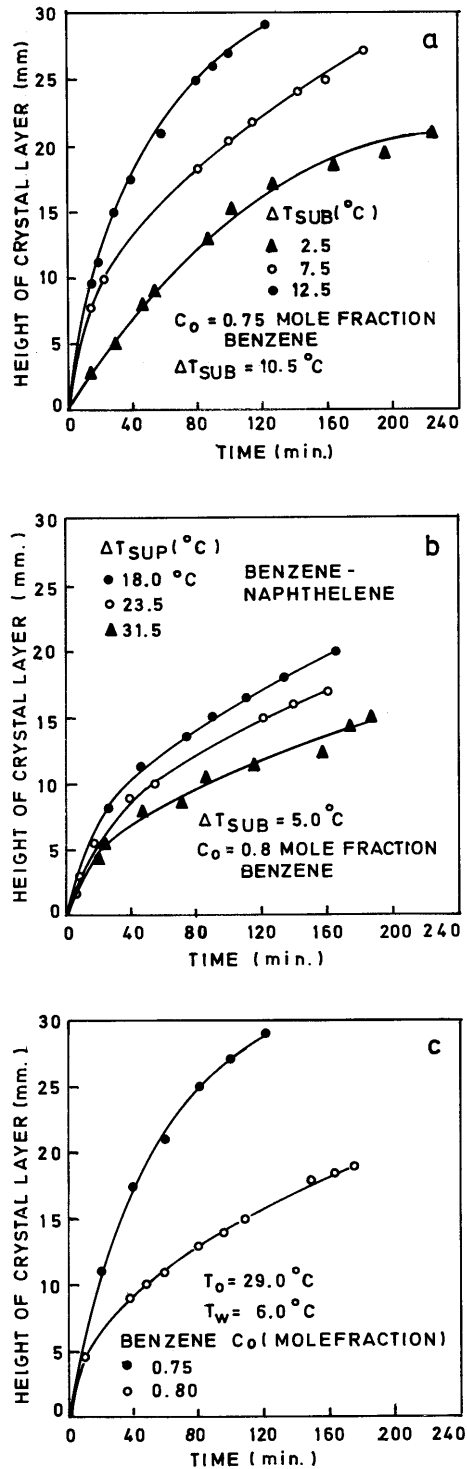


Fig. 5. Crystal growth rate of the benzene–naphthalene system, (a) effect of subcooling; (b) effect of initial superheat; (c) effect of initial concentration.

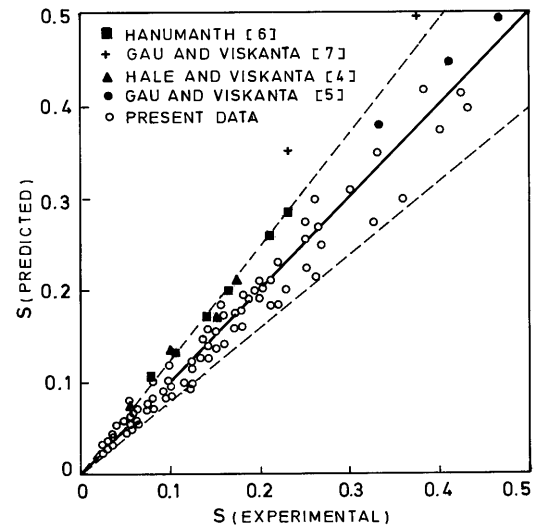


Fig. 6. Performance of the correlation for estimating the fractional (compared with initial) height of the crystallized material.

The present correlation under the limiting conditions of no initial superheat and for pure substances (that is  $C_0$  is 0) was compared with the data of Hanumant [6] on the solidification of n-hexadecane in a rectangular enclosure with cooling at the top surface in Fig. 6. The correlation was found to overpredict the data of Hanumant [6] by about 25%. This is due to the dominant natural convection effects that occur when the cooling is from the top. This natural convection in the liquid melt retards the growth of the crystal/melt interface.

Gau and Viskanta's [7] experimental data on the solidification of Lipowitz metal (an alloy of Bi, Pb, Sn and Cd) in a rectangular enclosure with no initial superheat and at its eutectic composition ( $Ste^* = 0$  and  $C'_0 = 0$ ) is shown in Fig. 6. The correlation overpredicts the data by about 30%. This is attributed to the initial mixing of their experiments, which would have had a retarding effect on the crystal growth. The correlation has also been compared with the data of Hale and Viskanta [4], who studied the freezing and melting of n-octadecane in a rectangular enclosure (again with  $Ste^* = 0$  and  $C'_0 = 0$ ) with slightly better agreement than with the data of Gau and Viskanta [7]. Gau and Viskanta's [8] experimental data on the solidification of pure gallium on a vertical wall with initial superheat is also shown in Fig. 6. Gau and Viskanta [8] studied the solidification in a rectangular enclosure with freezing from one of the vertical walls. The correlation appears to show good agreement with this data, the overprediction being less than 10%. The overprediction may be attributed to natural convection that will exist if the freezing surface is one of the vertical walls. This will have a retarding effect on the solid layer growth. In using the data of Gau and Viskanta [8] with the present

correlation,  $C'_0$  is set equal to 0 (pure substance). The total number of data points shown in Fig. 6 is about 200 including the present data. The present data matches the correlation within  $\pm 20\%$  and S.D. = 0.08.

Huppert and Worster [9] stated that the crystal layer height varied with the square root of the growth time. The present correlation also shows a similar dependence. Tanny [10] also reported a similar dependence for the diameter of a growing crystal. The present correlation with the exponent of the dimensionless time being 0.5 indicates the existence of a morphologically stable interface. On the other hand, according to Tanny [10], the exponent would have been closer to 0.7 if the interface had a spiky form.

#### 4.2. Average growth rate of crystal layer

A correlation has been developed for the average growth rate of the crystal layer in dimensionless form from the time required for growth to level off asymptotically. The crystal growth height versus time data from the experiments were fitted by a second order polynomial and differentiated to determine the instantaneous crystallization rate. The average crystallization velocity was obtained by integrating this instantaneous crystallization velocity over the time required for it to level off asymptotically. Subsequently, the average crystallization velocity is non-dimensionalised in terms of a Peclet number defined as

$$Pe = \frac{V_{cr}\delta}{D} \quad (7)$$

where,  $V_{cr}$  is the average crystallization velocity,  $\delta$  is the boundary layer thickness where a concentration and temperature gradient exists. The boundary layer thick-

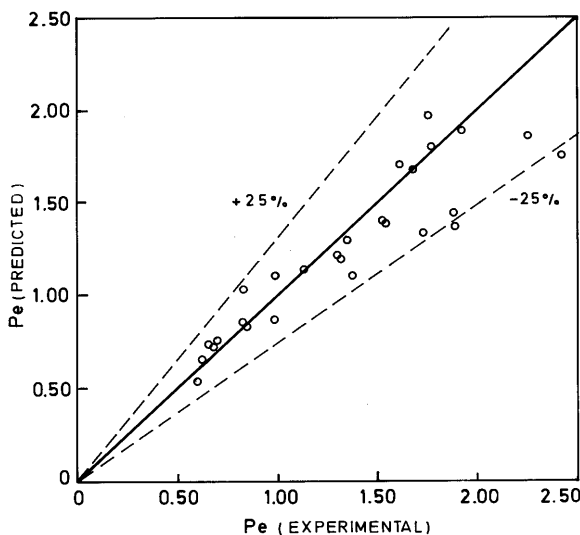


Fig. 7. Performance of the correlation for the average crystal growth velocity (velocity of the melt/crystal interface).

ness  $\delta$  is determined using the approach of Zief and Wilcox [11], who analyzed the free convection mixing during zone melting of organics in vertical glass tubes and this is given by

$$\delta = \frac{aR}{|F|(R/l)^{0.44}(V_{cr}l/D)^{0.26}} \quad (8)$$

where,  $a = 66$  when the interface density > bulk density of the melt. The parameter  $F$  is obtained from

$$F = Pr^{-0.25}Sc^{0.25} \left[ Gr + \left( \frac{Pr}{Sc} \right)^{1/2} Gr' \right]^{0.25} \quad (9)$$

for  $Pr < Sc$ . To use the above equation, the interface concentrations are required to determine  $Gr'$ , the mass transfer Grashof number. The interface concentration is obtained from an equation due to Huppert and Worster [9] for  $(D/\alpha)^{1/2} \ll 1$  and is given by

$$\left[ 1 + \frac{\psi C_0}{(T_i(C_0) - T_w)} \right]^{-1} = \frac{C_i - C_0}{C_0} \quad (10)$$

where,  $\psi$  is the slope of the phase diagram at the initial composition of the melt  $C_0$ , and  $C_i$  is the interface composition. The mass transfer Grashof number is defined as

$$Gr' = \frac{(gR^3\alpha')(x_i - x_{bl})}{v_m^2} \quad (11)$$

where,

$$\alpha' = \left( \frac{1}{\rho_m} \right) \left( \frac{\partial \rho_m}{\partial x} \right)_T \quad (12)$$

and the Grashof number is given by

$$Gr = \frac{(gR^3\beta')(T_i - T_{bl})}{v_m^2} \quad (13)$$

where,

$$\beta' = \left( \frac{1}{\rho_m} \right) \left( \frac{\partial \rho_m}{\partial T} \right)_x \quad (14)$$

The average crystallization velocity so obtained in terms of the Peclet number is correlated with the experimentally obtained crystallizing conditions such as Stefan number, the modified Stefan number (a dimensionless superheat) and the initial concentration as

$$Pe = 6.46Ste^{0.6}(1 - Ste^*)^{0.26}(C'_0)^{-0.11} \quad (15)$$

The performance of the correlation is shown in Fig. 7. The ranges of parameters are

$$0.022 < Ste < 0.12 \quad 0.13 < Ste^* < 0.413$$

$$0.086 < C'_0 < 0.92$$

The correlation predicts the experimental data within  $\pm 25\%$  and with S.D. = 0.26. It is seen that the Peclet

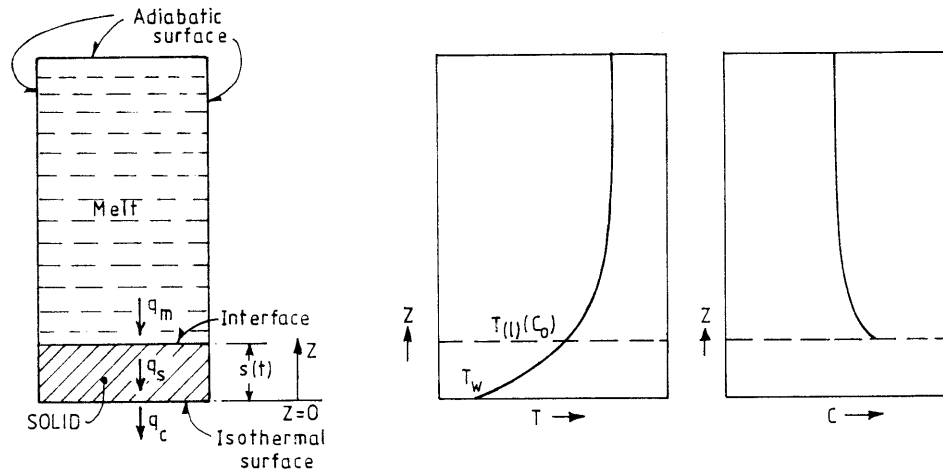


Fig. 8. Co-ordinates of the system for analysis.

number depends on the subcooling raised to the power of 0.6. Matsuoka et al. [12] observed a square root dependence while studying solidification rates. Similar dependency of the average crystal growth rate on subcooling was noticed by Libby and Chen [13] while studying the condensation of a gas stream on a cold surface.

### 5. Theoretical analysis of experimental data

Consider a binary melt of sub-eutectic composition at a temperature above its equilibrium temperature at that composition in a cylindrical container as used in the experimental part of this study and described earlier. The co-ordinates of the physical system are shown in Fig. 8. It is assumed that the solid/melt interface remains flat and parallel to the bottom surface. The transport of heat and solute takes place by molecular diffusion only. Heat is conducted through the liquid melt towards the interface and from there towards the cooling surface through the solid crystal layer. The solute diffusion takes place in the melt zone and that in the crystal region is neglected. The governing equations for heat transport in one-dimension are:

$$\frac{\partial T}{\partial t} = \alpha_s \frac{\partial^2 T}{\partial z^2} \quad (16)$$

in the solid zone  $0 < z < s(t)$  and

$$\frac{\partial T}{\partial t} = \alpha_m \frac{\partial^2 T}{\partial z^2} \quad (17)$$

in the melt zone  $z > s(t)$ .

The governing equation for solute transfer in the melt zone  $z > s(t)$  is given by

$$\frac{\partial C}{\partial t} = D \frac{\partial^2 C}{\partial z^2} \quad (18)$$

The boundary conditions are:

$$T = T_w \text{ at } z = 0, \quad t > 0$$

$$T = T_0 \text{ at } z \rightarrow \infty, \quad t > 0$$

$$C = C_0 \text{ at } z \rightarrow \infty, \quad t > 0$$

The initial conditions are  $T = T_0$  and  $C = C_0$  at  $t = 0$ . A heat balance at the interface at  $z = s(t)$  gives the heat flux which results from the latent heat released on solidification

$$\rho_s \lambda \frac{\partial s(t)}{\partial t} = k_s \left. \frac{\partial T}{\partial z} \right|_{(s^-, t)} - k_m \left. \frac{\partial T}{\partial z} \right|_{(s^+, t)} \text{ at } z = s(t) \quad (19)$$

where,  $\lambda$  is the latent heat of fusion and  $s^+$  and  $s^-$  represent the regions immediately adjacent to the interface of the liquid melt and the solid crystal, respectively. Conservation of the solute at the interface gives

$$C \frac{\partial s(t)}{\partial t} = -D \frac{\partial C(s^+, t)}{\partial z} \text{ at } z = s(t) \quad (20)$$

The solute diffusivity  $D$ , the thermal conductivity  $k$ , density  $\rho$  and the specific heat  $Cp$  are considered to be constant in each phase but different in the two phases. Solution of Eqs. (16)–(20) gives the temperature and the concentration fields in the two phases. Huppert and Worster [9] solved these equations and the results are

$$T(z, t) = T_w + (T_i - T_w) \frac{\text{erf}(\epsilon_s \eta)}{\text{erf}(\epsilon_s \gamma)} \quad (21)$$

in the domain  $z < s(t)$ .

$$T(z, t) = T_0 + (T_i - T_0) \frac{\text{erfc}(\epsilon_m \eta)}{\text{erfc}(\epsilon_m \gamma)} \quad (22)$$

in the domain  $z > s(t)$ .

$$C(z, t) = C_0 + (C_i - C_0) \frac{\operatorname{erfc}(\eta)}{\operatorname{erfc}(\gamma)} \quad (23)$$

in the domain  $z > s(t)$ . And  $\epsilon_m = (D/\alpha_m)^{1/2}$ ,  $\epsilon_s = (D/\alpha_s)^{1/2}$ ,  $\eta = 1/2(Dt)^{-1/2}z$ . The thermal diffusivity of the crystal phase and the melt phase are given by  $\alpha_s$  and  $\alpha_m$ , respectively. The parameter  $\gamma$  is given by Huppert and Worster [9] as

$$\psi C_0 \left[ \frac{F(\gamma)}{1 - F(\gamma)} \right] \left[ \frac{\rho_m C p_m}{F(\epsilon_m \gamma)} + \frac{\rho_s C p_s}{G(\epsilon_s \gamma)} \right] = \frac{\rho_s C p_s (T_i(C_0) - T_w)}{G(\epsilon_s \gamma)} - \frac{\rho_m C p_m (T_0 - T_i(C_0))}{F(\epsilon_m \gamma)} \quad (24)$$

where,

$$F(x) = \Pi^{1/2} x e^{x^2} \operatorname{erfc}(x) \quad (25)$$

and

$$G(x) = \Pi^{1/2} x e^{x^2} \operatorname{erfc}(x) \quad (26)$$

The interface concentration is obtained from the following equation

$$F(\gamma) = \frac{C_i - C_0}{C_0} \quad (27)$$

and subsequently the interface temperature is obtained from the phase diagram.

In order to use the above solutions due to Huppert and Worster [9], the parameter  $\gamma$  was determined from Eq. (24), using the experimental conditions encountered in each run in the present study together with the physical and transport properties of each binary mixture. It is then used in the form of  $F(\gamma)$  to estimate the interface concentration from Eq. (27). The values of  $F(\gamma)$  obtained from the conditions encountered in all the runs of the present experiments were in the range 0.001–0.1, indicating that the interface concentration,  $C_i$ , was extremely close to the initial concentration,  $C_0$  (Eq. (27)). This means that the interface temperature does not vary appreciably with the equilibrium temperature corresponding to the initial concentration of the melt (as obtained from the phase diagram).

As cooling proceeds, phase change will occur when the temperature of the melt reaches the equilibrium temperature corresponding to the concentration at the interface, which has been shown at or close to the initial concentration of the melt. Using Eq. (22), the temperature profile in the melt region has been estimated at different time instants for each run. Representative plots of the system benzene–naphthalene are shown in Fig. 9 for two time instants. Similar profiles were obtained for the other two systems also. The height obtained from the melt temperature profile at the equilibrium temperature corresponding to the initial concentration is shown by point one in the figures. The interface heights measured at different times during each run matched exactly with the height obtained from the temperature profile. This shows that the interface temperature does not vary significantly with the equilibrium temperature corresponding to the initial concentration. It also shows the existence of near equilibrium freezing conditions without appreciable subcooling at the interface.

The instantaneous heights obtained from the temperature profile (Eq. (22)) corresponding to the equi-

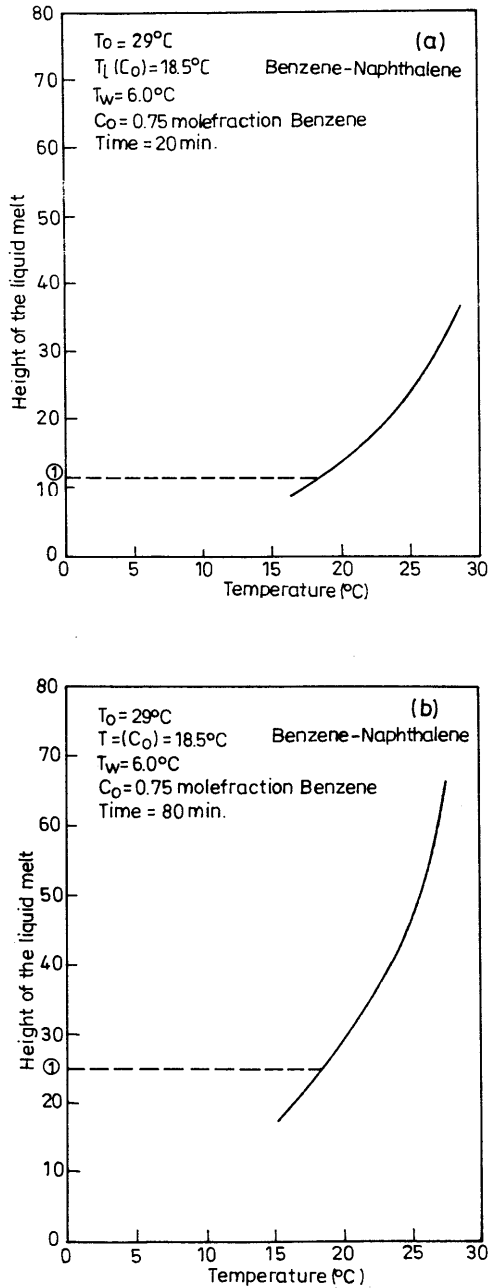


Fig. 9. Temperature profiles along the vertical direction estimated theoretically (Eq. (22)) for the benzene–naphthalene system, (a)  $t = 20$ ; (b)  $t = 80$  min.

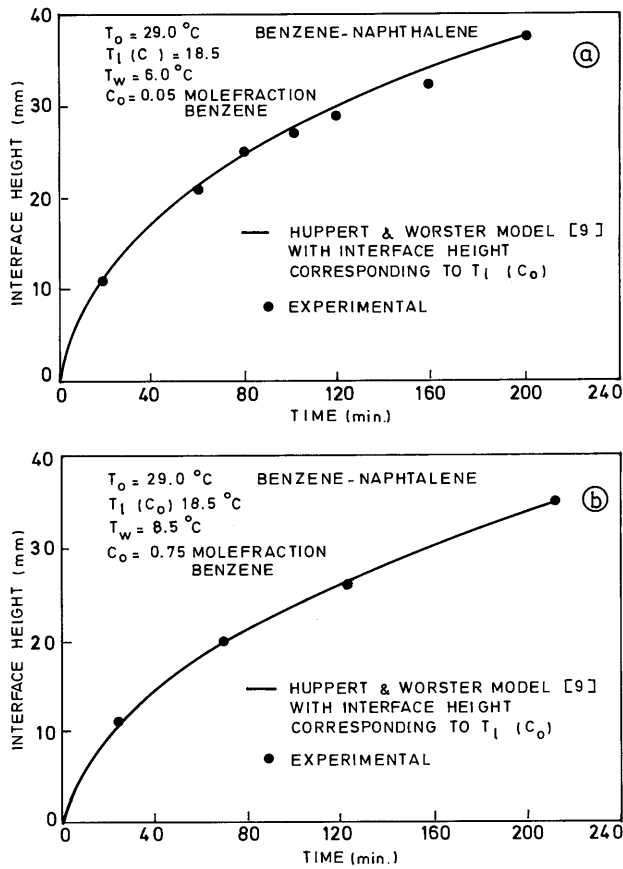


Fig. 10. Comparison of the measured interface heights with theory (Eq. (22)) corresponding to  $T_l(C_0)$  for the benzene–naphthalene system, (a)  $T_w = 6$ ; (b)  $T_w = 8.5^\circ\text{C}$ .

Equilibrium temperature of the melt at the initial concentrations are shown in Fig. 10 for different wall temperatures for the system benzene–naphthalene. The experimentally measured interface heights are also shown in the figure. It can be seen that there is good agreement between the present experimental data and the theoretical heights obtained. Similar agreement was noticed with the other two systems used in the present study.

## 6. Summary

The crystallization of a sub-eutectic binary mixture has been studied both experimentally and analytically. Under the conditions investigated, the systems were thermally stable and buoyancy induced motion in the melt zones was not noticed. The crystal/melt interface was flat, planar and morphologically stable. A one-dimensional moving boundary model for the solidification of pure substances from the literature was used to describe the process. In comparison to the experimental data, it was found that the interface concentration was close to the initial concentration of the melt. Using the

equilibrium temperature corresponding to the initial concentration, the solidification height was obtained which matched with the experimentally obtained interface height. The experimental data shows that the degree of subcooling, superheating and the initial concentration of the melt influence the rate of crystallization. The instantaneous crystal height and the average crystallization velocity vary approximately with the square root of time and degree of subcooling. Based on the present data a correlation has been proposed for the instantaneous crystal/melt interface height in melts cooled from below. The correlation has been validated with literature data for the limiting conditions of no superheat and for pure components.

## 7. Nomenclature

$C$	composition of the melt (mol%)
$C_p$	specific heat (J/(kg K))
$D$	mass diffusivity ( $\text{m}^2/\text{s}$ )
$F$	parameter in Eq. (21) (–)
$Gr$	Grashof number (heat transfer), $g\beta'R^3(T_i - T_{bi})/v^2$ (–)
$Gr'$	Grashof number (mass transfer), $g\alpha'R^3(x_i - x_{bi})/v^2$ (–)
$k$	thermal conductivity (W/(m K))
$l$	height of melt (initial) (m)
$Pe$	Peclet number (defined by Eq. (7)) (–)
$Pr$	Prandtl number, $v/\alpha$ (–)
$R$	radius of the cylinder (m)
$R'$	pseudo steady state velocity of the interface (m/s)
$s$	height of the interface (m)
$S$	dimensionless height of the interface (m)
$Sc$	Schmidt number, $v/D$ (–)
$Ste$	Stefan number, $Cp_s(T_l(C_0) - T_w)/\lambda$ (–)
$Ste^*$	modified Stefan number, $Cp_m(T_o - T_l(C_0))/\lambda$ (–)
$t$	time (s)
$T$	temperature ( $^\circ\text{C}$ )
$T_l(C_0)$	liquidus temperature corresponding to $C_0$ ( $^\circ\text{C}$ )
$V_{cr}$	average crystallization velocity (m/s)
$x$	co-ordinate in the direction of crystal growth (m)
$x$	composition of the melt (mol%)
$X$	dimensionless height, $x/l$ (–)
$\Delta T_{sub}$	subcooling of the melt, $(T_l(C_0) - T_w)$ (K)
$\Delta T_{sup}$	initial superheat of the melt, $(T_o - T_l(C_0))$ (K)
<i>Greek symbols</i>	
$\alpha$	thermal diffusivity ( $\text{m}^2/\text{s}$ )
$\alpha'$	volumetric coefficient of concentration expansion ( $1/(\text{mol}\%)$ )

$\beta'$	volumetric coefficient of thermal expansion (1/K)
$\gamma$	parameter used in Eq. (4) (–)
$\delta$	parameter used in Eq. (5) (–)
$\delta$	parameter used in Eq. (20) (m)
$\varepsilon$	porosity or void fraction (–)
$\theta$	dimensionless temperature, $(T - T_w)/(T_0 - T_w)$ (–)
$\lambda$	latent heat of fusion (J/kg)
$\nu$	kinematic viscosity (m <sup>2</sup> /s)
$\xi$	slope of the liquidus line
$\rho$	density (kg/m <sup>3</sup> )
$\rho^*$	bulk density of the crystals (kg/m <sup>3</sup> )
$\tau$	dimensionless time, $\alpha_s t/l^2$ (–)
$\psi$	parameter defined in Eq. (24)

### Subscripts

bl	bulk
e	eutectic
i	interface
m	melt
0	initial value
s	solid (crystal)
w	wall (surface)

### References

- [1] N.P. Wynn, Separate organics by melt crystallization, Chem. Eng. Prog. 88 (1992) 52–60.
- [2] J. Ulrich, Melt crystallization, in: A. Myerson (Ed.), Industrial Crystallization, Butterworth/Heinemann, London, 1994, pp. 151–164.
- [3] S. Rittner, R. Steiner, Melt crystallization of organic substances and its large scale applications, Chem. Ing. Tech. 57 (1985) 91–102.
- [4] N.W. Hale, Jr, R. Viskanta, Solid–liquid phase change heat transfer and interface motion in materials cooled or heated from above or below, Int. J. Heat Mass Transfer 23 (1980) 283–292.
- [5] M.G. Worster, Solidification of an alloy from a cooled boundary, J. Fluid Mech. 167 (1986) 481–501.
- [6] G.S. Hanumanth, Solidification in the presence of natural convection, Int. Commun. Heat Mass Transfer 17 (1990) 283–292.
- [7] C. Gau, R. Viskanta, Melting and solidification of a melt system in a rectangular cavity, Int. J. Heat Mass Transfer 27 (1984) 113–123.
- [8] C. Gau, R. Viskanta, Melting and solidification of a pure metal on a vertical wall, ASME J. Heat Transfer 108 (1986) 174–181.
- [9] H.E. Huppert, M.G. Worster, Dynamic solidification of a binary melt, Nature 314 (1985) 704–707.
- [10] J. Tanny, Experimental study on the crystallization of a binary melt at the vertical boundary of an enclosure, Int. J. Heat Mass Transfer 38 (1995) 1141–1150.
- [11] M. Zief, R. Wilcox, Fractional Crystallization, Marcel Dekker, New York, 1967, pp. 61–62.
- [12] M. Matsuoka, T. Fukuda, Y. Takagi, H. Takiyama, Purification by sweating of organic solid solutions by layer and suspension type melt crystallization operations, J. Chem. Eng. Jpn. 28 (1995) 562–569.
- [13] P.A. Libby, S. Chen, The growth of a deposited layer on a cold surface, Int. J. Heat Mass Transfer 8 (1965) 395–402.